Journal of Hydrology 594 (2021) 125792

Contents lists available at ScienceDirect

Journal of Hydrology

journal homepage: www.elsevier.com/locate/jhydrol

Research papers

Factors controlling discharge-suspended sediment hysteresis in karst basins, southwest China: Implications for sediment management

Le Cao [a,b,c], Shuang Liu [h], Shijie Wang [a], Qianyun Cheng [a,c], Alan E. Fryar [g], Lin Zhang [a,d], Zhicai Zhang [e], Fujun Yue [f], Tao Peng [a,d,*]

[a] State Key Laboratory of Environment Geochemistry, Institute of Geochemistry, Chinese Academy of Sciences, Guiyang 550081, China
[b] Center for Lunar and Planetary Sciences, Institute of Geochemistry, Chinese Academy of Sciences, Guiyang 550081, China
[c] University of Chinese Academy of Sciences, Beijing 100049, China
[d] Puding Karst Ecosystem Research Station, Chinese Academy of Sciences, Puding 562100, China
[e] State Key Laboratory of Hydrology-Water Resources and Hydraulic Engineering, College of Hydrology and Water Resources, Hohai University, Nanjing 210098, China
[f] Institute of Surface-Earth System Science, Tianjin University, Tianjin 300072, China
[g] Department of Earth and Environmental Sciences, University of Kentucky, 101 Slone Building, Lexington, KY 40506-0053, United States
[h] Institute of Geology, Hunan University of Science and Technology, Xiangtan 411201, China

ARTICLE INFO

This manuscript was handled by Corrado Corradini, Editor-in-Chief, with the assistance of Jongjun Jiang, Associate Editor

Keywords:
Karst
Hysteresis analysis
Turbidity
Suspended sediment transport
Ground substance component

ABSTRACT

Assessment of river sediment sources, transport, and controlling factors in karst regions is critical to the development of effective soil erosion and sediment management strategies. This 2-year study used a hysteresis index of discharge and suspended sediment data, combined with the basin's inherent geological characteristics, to assess sediment sources and hydrological connectivity at six sites in an agricultural karst watershed of southwest China. Principal component analysis was further used to describe sediment control by rainfall (antecedent precipitation, precipitation duration, amount, and intensity) and stream hydrology (maximum and total discharge, flood intensity, and runoff coefficient). Results indicate that the annual sediment yield (0.8–6.6 Mg km^2 a^{-1}) is low and sediment transport in karst areas is dependent on continuous rainfall. Ground substance component (GSC) and geomorphology characteristics determine the hydrology connectivity and sediment availability. In a sub-basin (CQ) marked by a peak cluster depression with good vegetation, sediment mainly comes from the paddy land, and the surface stream shows clockwise hysteresis. During storms, surface water enters the underground system from sinkholes, resulting in Figure-8 hysteresis with multiple sediment peaks. In another predominantly agricultural sub-basin (HTP), the thick layers of paddy and loess soil surrounding the river channel provide an accessible sediment source, resulting in clockwise hysteresis. The surface outlet of the watershed (HZ) is affected by an upstream reservoir, but bank erosion and sediment activation are evident during storms. The subsurface outlet (MSK) of the watershed shows more anti-clockwise hysteresis due to the activation of the conduit network in the wet season, surface water draining into the underground river and the distant sediment sources. This study shows that discharge-suspended sediment concentration hysteresis analysis can provide a reference for soil and water conservation decision-making in karst areas.

1. Introduction

Soil erosion and river sediment transport have become serious social and environmental problems all over the world. Excessive sediment entering a river will reduce its ecological function, and sediment-related substances, such as phosphorus, can also have a negative impact on water quality (Krueger et al., 2009). River suspended-sediment concentration (SSC) can reflect the regional soil erosion. Therefore, it is very important to evaluate the source, transport and controlling factors of river SSC for implementing effective soil erosion and sediment management strategies (Li et al., 2017).

Karst areas in southwest China are likely to suffer from soil erosion due to their special geological background (vast soluble carbonate rocks), humid climate and dense agricultural population (Wang et al., 2003). Compared to non-karst areas, this area has large surface fluctuation, low surface runoff coefficient, shallow and discontinuous soil. In

* Corresponding author at: State Key Laboratory of Environment Geochemistry, Institute of Geochemistry, Chinese Academy of Sciences, Guiyang 550081, China.
E-mail address: pengtao@mail.gyig.ac.cn (T. Peng).

https://doi.org/10.1016/j.jhydrol.2020.125792

Available online 26 November 2020

addition to soil erosion on the surface, the development of solution-enhanced conduits leads to underground soil leakage (Zhang et al., 2007). Due to the close relationship between karst soil erosion and rocky desertification, scientific research has been carried out on soil erosion and land degradation, environment factors, characteristics and its occurrence law in the process of karst rocky desertification (He et al., 2009). The surface soil erosion in the carbonate rock area significantly changes with seasonal precipitation (Bai and Wan, 1998). On macro-scale, geological structure affects the distribution of surface material and surface runoff by controlling the characteristics of landforms, thus affecting soil erosion (Huaduan and Rui, 2006). The forest vegetation coverage rate in karst areas is usually lower than that in non-karst areas, which also reduces the functions of vegetation on soil water conservation, soil consolidation and fixation (Cao et al., 2003). What is more, modern erosion is a comprehensive process of natural erosion and man-made accelerated erosion. Based on the previous studies, Zhang put forward the view that soil erosion on karst slopes is a mixture of surface water erosion, gravity erosion, chemical dissolution, underground erosion, creep, and man-made accelerated erosion (Zhang et al., 2007).

At present, some methods have been used to study the sediment sources and transport in karst areas (Chen et al., 2017; Li et al., 2016; Saleh, 2008; Vigiak et al., 2017; Gao et al., 2013). Cheng et al. (2020) used fingerprint tracing to investigate sediment sources in a karst landscape, and pointed that subsurface and clastic rock sources represent a significant component of the catchment sediment budget, targeting hillslope surface soils alone may have limited impact on suspended sediment export at landscape scale. Li et al. (2020) used a composite fingerprinting to investigate sediment sources and their relative contributions in a karst depression, they pointed out that soil conservation measures are required to control soil erosion for cropland due to its high sediment contribution, and great attention should be paid when using only a single core to quantify sediment provenance. Li et al. (2016) used a revised universal soil loss equation (RUSLE) for estimating the spatial and temporal distribution of soil erosion, and result shows that the intensity level of soil erosion changes across space. The most active area is mainly concentrated in the upstream peak cluster depression. However, the application of these methods is limited by their high requirements of sample representativeness and sample quantity.

With the development of monitoring technology, the acquisition of high resolution discharge and sediment monitoring data has become simple, and the explanation of discharge-suspended sediment concentration (Q-SSC) hysteresis can provide another way to understand the changes of sediment sources, sediment reserves and flow pathways (Sherriff et al., 2016; Vercruysse et al., 2017). Many versions of the hysteresis index (HI) have been developed to describe the types of hysteresis, which is helpful for quantitative description and comparative analysis of time-varying storm events in multiple basins (Langlois et al., 2005; Lloyd et al., 2016). This method (Q-SSC hysteresis analysis) had proven reliable in many areas (Langlois et al., 2005; Sherriff et al., 2016), but which had not yet been used for sediment management studies of karstic water systems in China.

In order to develop a targeted sediment management plan, it is necessary to develop a comprehensive understanding of water and sediment control factors in karst agricultural basins. The objectives of this study were to: (1) determine the main sediment transport channels and their source areas based on the analysis of Q-SSC hysteresis and data on hydrogeology, soil and land use; (2) deduce the potential factors controlling sediment transport based on the mathematical analysis of the characteristics of sediment transport and rainfall, runoff and antecedent rainfall; (3) provide advice on sediment management for different basins.

2. Materials and methods

2.1. Study area

The study area is located in the Houzhai River catchment in Guizhou province China, in the center of the Southeast Asian karst region (Fig. 1). As of 2010, about 32,400 people lived in the Houzhai catchment, and more than 95 percent of the population worked in agriculture. The catchment is therefore thought to be experiencing land-use disturbance (Li et al., 2010).

The Houzhai catchment is classified as a typical mountain karst river basin (Wang and Zhang, 2001). The elevation is between 1210 and 1565 m above sea level, with a decreasing trend from southeast to northwest (Fig. 2 (A)). The change trend of landform from upstream to downstream is peak-cluster depression, peak-cluster valley, peak-forest basin and peak-forest plain. The lithology consists of the Middle Triassic Guanling Formation, with limestone, dolomite, pelitic dolomite and thin marl (Fig. 2 (B)). The upper reaches of the basin are mainly composed of depressions and peak forests (Fig. 2 (D)), with few surface water systems and developed underground water systems. The potential energy of groundwater is large, the flow velocity is fast, and the water transformations (precipitation, surface water and ground water) are rapid. Due to the lack of residual materials or deposits transported by external forces, the soil is generally composed of black and yellow lime soil formed by in-situ weathering. The middle reaches of the basin can be divided into two sub regions of different geomorphology and landscape (Fig. 2 (D)). The northern part is a dolomite marl area with undeveloped underground structure. The landform combination of this area is peak-forest karst plain, and the residual peak forest with tens of meters high is distributed in island cluster. The hydraulic gradient is small (4.2‰ to 7.8‰), the surface water system flow direction is not concentrated. There are some ancient river channels and dry valleys. Influenced by lithology (dolomite and calcareous dolomite), the red weathering crust platform is formed, and the gently ground covered by thick loose laterite soil layer. The southern part of the middle reaches of the basin is peak-forest valley area. The peak forest is distributed in the form of clan or island. The vertical seepage zone is small, the groundwater depth is shallow (3 to 12 m), and the surface river alternates with the underground river. The surface is flat (7‰ average hydraulic gradient) with many springs. Black and yellow limestone soil is distributed on the slopes, paddy soil is distributed on the dam lands. The residual red clay (7 to 8 m thick) accounts for 20% of the area. The lower reach of the basin is peak-cluster and hilly combination type landform (Maokeng to MSK) (Fig. 2 (D)). Due to the decrease of the base level of surface erosion, some areas are reactivated and many depressions and sinkholes are formed.

Houzhai River, which originates from Muzhu cave, is the main surface river in Houzhai basin (Fig. 2 (D)). Zhongba River and Dengzhan river flow into Houzhai River near HTP (Abbreviation of Huangtupo, place name), and flow out from northwest of basin after passing Qingshan Reservoir. Houzhai underground river originated in the East (Fig. 2 (D)). After the groundwater converges to the Muzhu reservoir, part of the groundwater continues to flow in the ground-system, passing through the LHT (Abbreviation of Laoheitan, place name) in the southwest, and finally flows out of the surface at MSK (Abbreviation of Maoshuikeng, place name); the rest of the groundwater flows into the northwest of the basin after converging with the surface tributaries from the northeast, and finally flows out of the basin from HZ (Abbreviation of Houzhai, place name) (Yue et al., 2015). The runoff at the outlet (HZ and MSK) accounts for more than 95% of the total runoff of the basin, and only a part of groundwater flows out of the basin at the southwest boundary. The surface river and underground river in Houzhai basin formed a unique “double layer” structure system through hydraulic connection. The basins were divided into sub-basins according to geomorphic types or landforms and hydrological stations were set up at the outlet of each basin. Table 1 shows the basic information of Houzhai

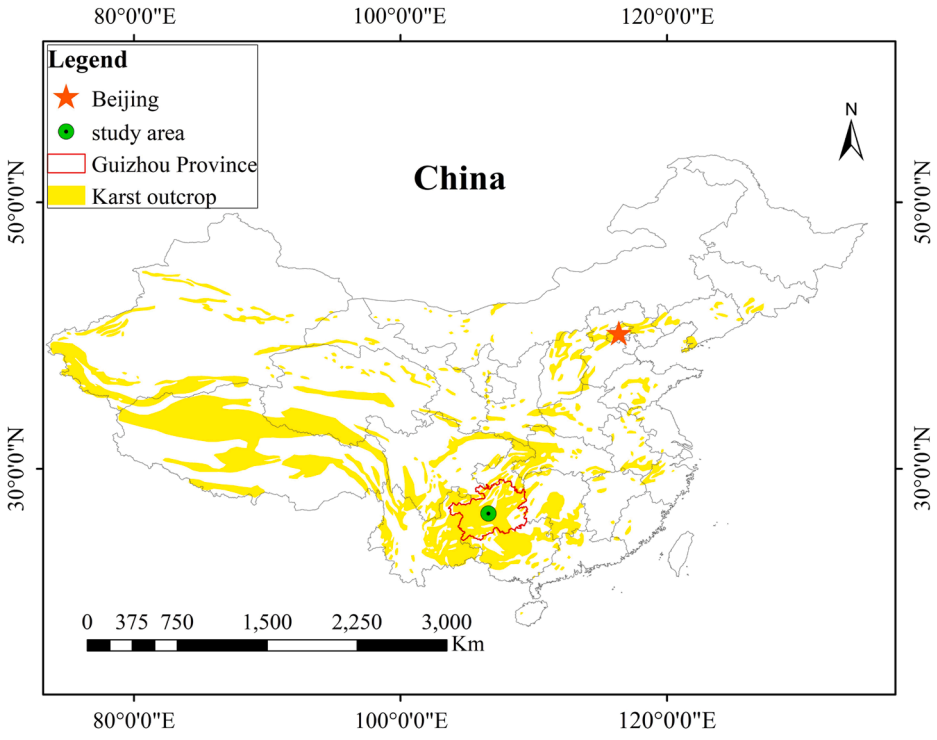

Fig. 1. Context map of China with karst outcrop in yellow and the Houzhai catchment indicated by the green circle.

and its sub-watershed hydrology stations.

2.2. Data collection

Suspended sediment data were collected at each hydrology station using high-resolution (10-min) turbidity (VisoTurb@700IQ, WTW, Xylem Analytics) and Q measurements. Turbidity was calibrated to SSC using a rating curve (Eder et al., 2010; Gippel, 1995). During storms, river water was collected in a 300-mL plastic bottle at 2-hour intervals. The suspended sediment concentration was measured by filtering the river water with a 0.45-μm filter membrane. This approach for SS estimation was validated by direct depth-integrated and cross-sectional samples and no differences in turbidity-SSC relationship occurred between event and nonevent samples (Sherriff et al., 2015; Yan et al., 2021). A total of 243 valid samples were collected during the storm events, and the turbidity-SSC relationship for each hydrological station is shown in Fig. 3 (CQDB, n = 41, R^2 = 0.93; CQDX, n = 36, R^2 = 0.71; HTP, n = 33, R^2 = 0.98; LHT, n = 33, R^2 = 0.72; HZ, n = 42, R^2 = 0.98; MSK, n = 42, R^2 = 0.94). Triangular rafts were installed at hydrological stations using HOBO U20 (Onset Computer) pressure transducers with a resolution of 0.02 kPa and a monitoring interval of 10 min. Measured water pressures were corrected for barometric pressure fluctuations and converted to water levels, from which flow rates were calculated using a rating curve. Meteorological data were collected from three weather stations (HOBO U30) measuring 10-min resolution rainfall, air temperature, relative air humidity, radiation and wind speed.

2.3. Data analysis

The individual storm events from January 2017 to December 2018 were extracted according to the suspended sediment characteristics of each hydrological station. In this study, a storm event is usually defined as having total precipitation (P) >10 mm and significant changes in Q and SSC. However, the parameters defining storms differ between watersheds (or hydrological stations). For CQDB, the start of a storm event is defined as the rate of change for 10 consecutive minutes >0.35 $m^3 s^{-1}$ for Q and 1.0 g m^{-3} for SSC measurements, and the end of the storm event is defined as a change in Q < 0.06 $m^3 s^{-1}$ in a continuous 6-hour measurement and SSC < 3 g m^{-3}. Table 2 shows the storm definition parameters for all hydrological stations and the number of storm events counted for each hydrological station.

Storm events are finally classified by hysteresis categories and HI. The hyperbolas of Q and SSC indicate the direction and qualitative type of hysteresis: clockwise, where SSC peaks before Q; anti-clockwise, where Q peaks before SSC; figure-8, with both clockwise and anti-clockwise characteristics; and indeterminate, in which the relationship between SSC and Q is difficult to define. Hysteresis index is a numerical indicator for each storm event calculated with Q and SSC data. HI_{new} is used in this study because it is more stable than other indicators and can provide a comparison between different watersheds (Lloyd et al., 2016). HI_{new} uses the difference between the SSC values on the rising limb (RL) and falling limb (FL) of a storm, rather than a ratio, and effectively normalizes RL and FL at every measurement point, thereby resulting in an index between − 1 and 1:

$$NormalizedQ_i = \frac{Q_i - Q_{min}}{Q_{max} - Q_{min}} \quad (1)$$

$$NormalizedSSC_i = \frac{SSC_i - SSC_{min}}{SSC_{max} - SSC_{min}} \quad (2)$$

$$HI_{new} = SSC_{RL\_norm} - SSC_{FL\_norm} \quad (3)$$

where the i subscript refers to timestep i, and min and max refer to the minimum and maximum storm parameter values, respectively. The analysis is carried out using 10% intervals of Q and the average value is used as the final HI_{new} value of the storm. A higher HI_{new} indicates a greater asynchronous behavior between SSC and Q. A positive HI_{new} indicates more clockwise hysteresis and a negative HI_{new} indicates more anti-clockwise hysteresis.

The data are classified according to hysteresis types (clockwise, anti-clockwise, figure-8, indeterminate) to facilitate the investigation of the control factors at each hydrological station. Sixteen potential control factors were collated for each sub-basin in individual storm events (Belmont et al., 2014; Sherriff et al., 2015). Discharge parameters

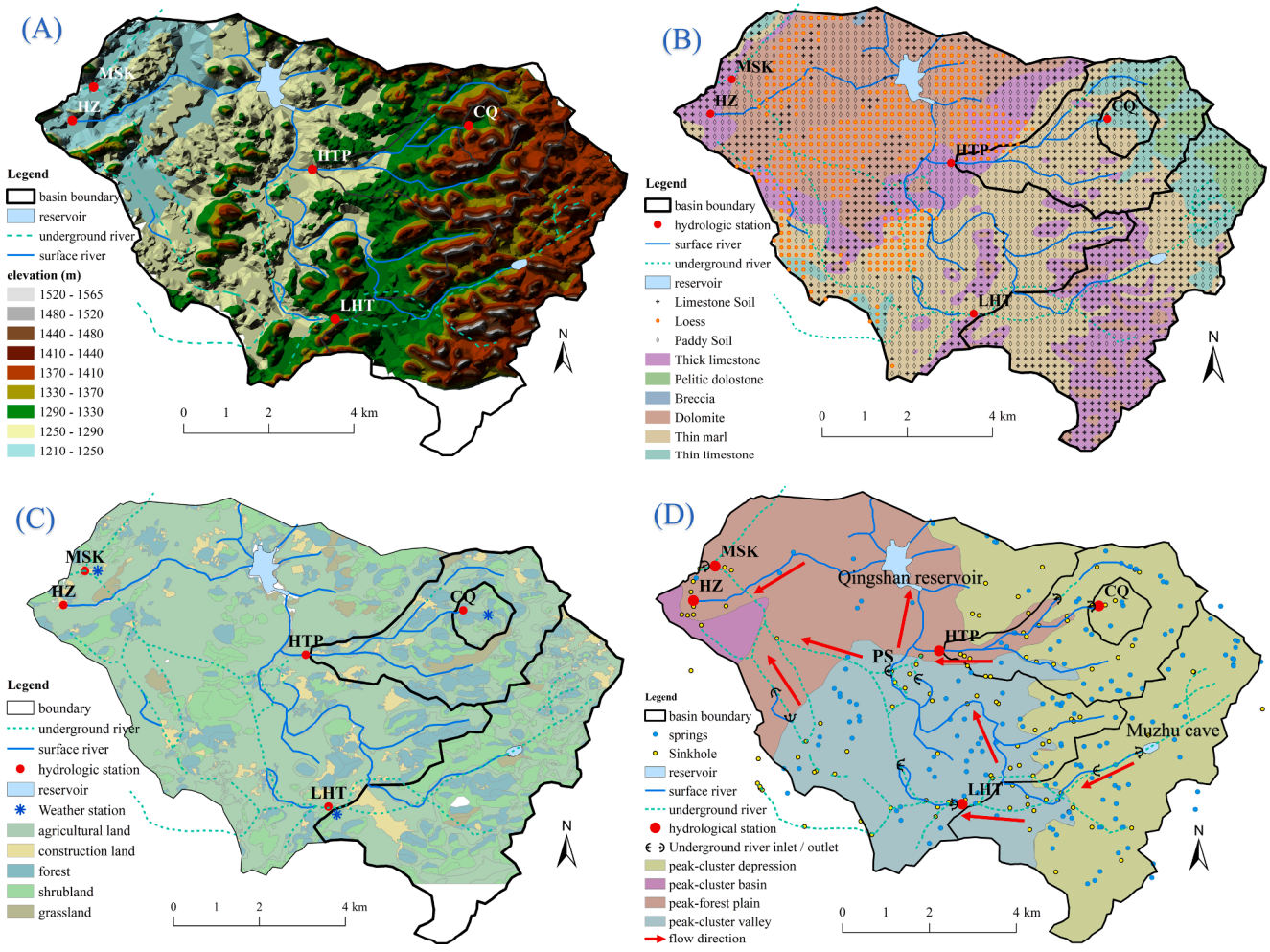

Fig. 2. Houzhai river basin and sub-basins (CQ, HTP, LHT): (A) Digital elevation model; (B) Soil and lithologic distribution; (C) Land usage; (D) Geomorphology and hydrology.

Table 1
Summary of study hydrological stations.

Hydrological stations	CQDB	CQDX	HTP	LHT	HZ	MSK
Catchment area (km^2)	1.26	1.26	10.97	16.15	73.39	73.39
River type	Surface	Underground	Surface	Underground	Surface	Underground
Soil type: dominant	Limestone soil (77%)	Limestone soil (77%)	Limestone soil (66%), paddy soil (28%)	Limestone soil (74%), paddy soil (22%)	Limestone soil (44%), paddy soil (35%)	Limestone soil (44%%), paddy Soil (35%)
minor	Paddy soil (14%)	Paddy soil (14%)	Loess (6%)	Mud soil (4%)	Loess (17%)	Loess (17%)
Land use	Slope land 34%, forest 28%, shrubland 25%	Slope land 34%, forest 28%, shrubland 25%	Paddy field 31%, forest 26%, slope land 20%	Paddy field 30%, shrubland 28%, forest 16%	Paddy field 47%, shrubland 17%, forest 16%	Paddy field 47%, shrubland 17%, forest 16%
Annual rainfall (mm)	869–1702 mm, average 1339 mm (1961–2005)					

include maximum discharge ($m^3\ s^{-1}$), total event discharge (Q_{total}, m^3), event duration (T, h), flood intensity (($Q_{max} - Q_{min}$) / time of rise), and rainfall-runoff ratio (%). Precipitation parameters include total event precipitation (P, mm), duration of rainfall event (T_{rain}, h), maximum precipitation intensity at 10- and 30-min resolutions (I_{10} and I_{30}, mm h^{-1}), and average precipitation intensity (I_{mean}, mm h^{-1}). Antecedent parameters include rainfall at 1, 3, 5, 7, and 10 days before event initiation (mm). SSC_{mean} (total event SS load divided by total event flow volume, g m^{-3}) was selected as the sediment response variable. This flow-weighted concentration index can better indicate the availability of the source by reducing the impact of basin hydrology, and it also eliminates any potential autocorrelation with the discharge parameters used to calculate SSC. Principal component analysis (PCA) is carried out for each main hysteresis type of each hydrological station, and the potential controls are defined as those that occupy similar areas of SSC_{mean} on the PCA loading map (Dominic et al., 2015; Sherriff et al., 2015; Tena et al., 2014).

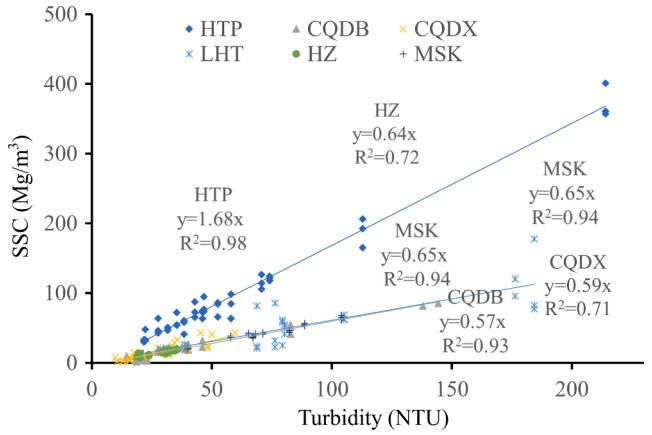

Fig. 3. Relationship between suspended sediment concentration (SSC) and turbidity at six stations.

Table 2
Definition of storm event initiation and termination in each station.

Station (number of storms)	Parameters defining storm event initiation		Parameters defining storm event termination	
	Q increase in 10 min	SSC increase in 10 min	Q reduction in 6 h	SSC <
CQDB (15)	0.10 $m^3 s^{-1}$	2.0 g m^{-3}	0.06 $m^3 s^{-1}$	3 g m^{-3}
CQDX (22)	0.02 $m^3 s^{-1}$	1.0 g m^{-3}	0.01 $m^3 s^{-1}$	2 g m^{-3}
HTP (8)	0.12 $m^3 s^{-1}$	20.0 g m^{-3}	0.10 $m^3 s^{-1}$	10 g m^{-3}
LHT (18)	0.03 $m^3 s^{-1}$	1.8 g m^{-3}	0.02 $m^3 s^{-1}$	2 g m^{-3}
HZ (13)	0.15 $m^3 s^{-1}$	9.0 g m^{-3}	0.10 $m^3 s^{-1}$	5 g m^{-3}
MSK (11)	0.24 $m^3 s^{-1}$	2.0 g m^{-3}	0.15 $m^3 s^{-1}$	4 g m^{-3}

3. Results

3.1. SS load at each station

Fig. 4 shows the daily SS load sequence of each hydrological station and the weekly rainfall distribution in Houzhai basin for 2017 and 2018 (HTP is only in 2018). There is a strong correlation between sediment transport volume and rainfall at each hydrological station, which also indicates that rainfall is the main external driving factor of soil erosion and sediment transport. The distribution of SS load is uneven: the wet season (May – September) accounts for more than 90% of the SS load, and SS load is mainly controlled by individual storm events (<10 per year). From CQ to HTP to HZ, the daily sediment transport gradually increases with the catchment area.Table 3

Table 4 shows the sediment and runoff information in each

Table 3
Inferring catchment hydro-geomorphic processes regulating sediment erosion and transport using Q-SSC hysteresis type (Belmont et al., 2014; Sherriff et al., 2015).

Hysteresis type	Proximal hydro-geomorphic processes (close to monitoring point or connected by rapid hydrological pathway)	Distal hydro-geomorphic processes (far from monitoring point or connected by delayed hydrological pathway)
Clockwise	High sediment quantity Re-suspension of bed sediment storage Eroding banks near monitoring point Surface erosion	Low sediment quantity Sources exhausted due to previous events High ground cover in fields Low connection between sources and outlet
Anti-clockwise	Low sediment quantity Proximal bed sediment sources exhausted due to previous events High channel bank vegetation High ground cover in proximal fields Limited channel bed scour	High sediment quantity Low ground cover in fields High compaction in fields High connectivity between distal sources and outlet High antecedent wetness
Figure-8 Indeterminate	Mixed with clockwise and anti-clockwise Dependent upon magnitude of sediment response High proximal and distal Moderate proximal and distal Low proximal and distal	

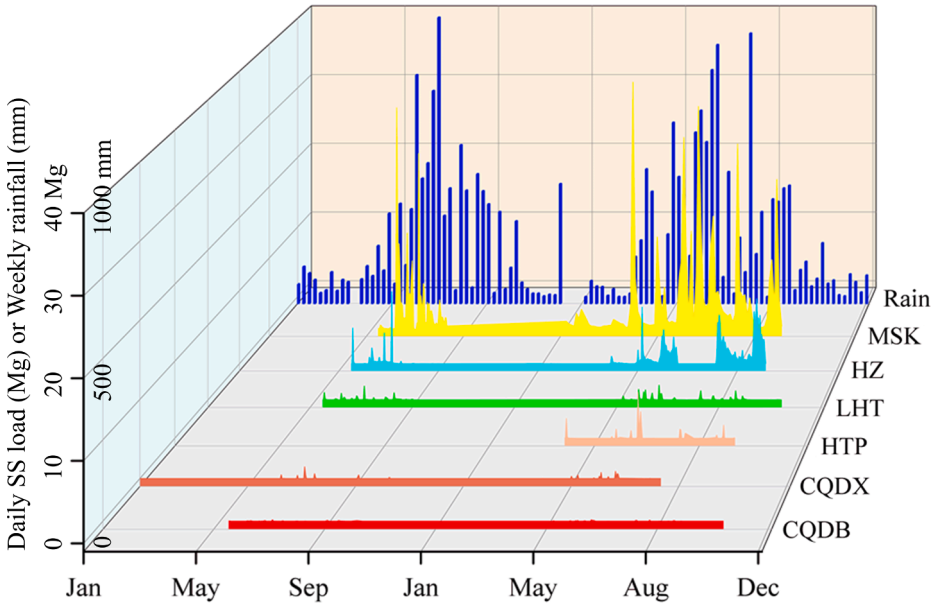

Fig. 4. Daily suspended sediment load (SS load) sequence of each hydrological station and the weekly rainfall distribution in Houzhai basin, 2017–2018.

Table 4
Statistical information of sediment runoff in each hydrological station.

	Total discharge, 10^6 m^3 (2017/2018)	Runoff coefficient (2017/2018)	Total SS load, Mg (2017/2018)	Sediment transport modulus, Mg km^{-2} a^{-1} (2017/2018)
CQDB	0.12/0.21	0.14/0.16	5.3/6.75	4.0/5.4
CQDX	0.14/0.26	0.15/0.16	1.3/1.35	1.1/1.2
HTP	0.53/0.65	0.05/0.06	–/32	–/2.9
LHT	7.32/7.55	0.41/0.35	14.6/24.4	0.8/1.3
HZ	8.74/8.88	0.08/0.10	134/117	1.8/1.6
MSK	22.2/33.9	0.28/0.26	335/485	4.5/6.6

hydrological station. 2018 was wetter than 2017 (1170 mm vs. 960 mm). Underground river flow in the Houzhai basin accounted for more than 70% of total runoff. CQ and Houzhai basins are closed, as reflected by runoff coefficients between 0.3 and 0.4. In the HTP basin, the runoff coefficient was <0.1, which indicates that there may be underground rivers or other outlets besides the monitored surface stream. The annual sediment transport modulus of Houzhai and its sub-basins ranged from 0.8 to 6.6 Mg km^{-2} a^{-1}.

3.2. Storm event hysteresis

Fig. 5 shows the distribution of HI_{new} in all storm events at six hydrological stations (four basins) over a 2-year period. From upstream to downstream within the Houzhai basin, HI_{new} has a trend from large to small and from more clockwise to more anti-clockwise. The average HI_{new} value of CQ, LHT, and HTP basins in the middle and upper reaches is between 0.27 and 0.39, but the average value of HZ and MSK in the lower reaches is 0.02 and −0.06, respectively. CQDB and CQDX have mainly clockwise hysteresis, in which CQDX shows the maximum value of HI_{new} in all basins (0.85). The SSC range of CQDB (average 129 g m^{-3}) is larger than that of CQDX (average 22 g m^{-3}). HTP is clockwise except for one anti-clockwise event, and the SSC of HTP is the largest of all drainage basins, reaching a maximum of 820 g m^{-3}. The HI_{new} values of LHT are all >0 and tend to be clockwise, but the SSC range at LHT is the smallest of all stations (average 18 g m^{-3}). MSK and HZ HI_{new} values are basically distributed around 0, which indicates that their hysteresis types are relatively complex. Their average SSC values (83 and 81 g m^{-3}, respectively) ranged in the middle of all hydrology stations. The SSC range of all underground rivers (CQDX, LHT, MSK) is significantly smaller than that of surface rivers (CQDB, HTP, HZ). The wet season

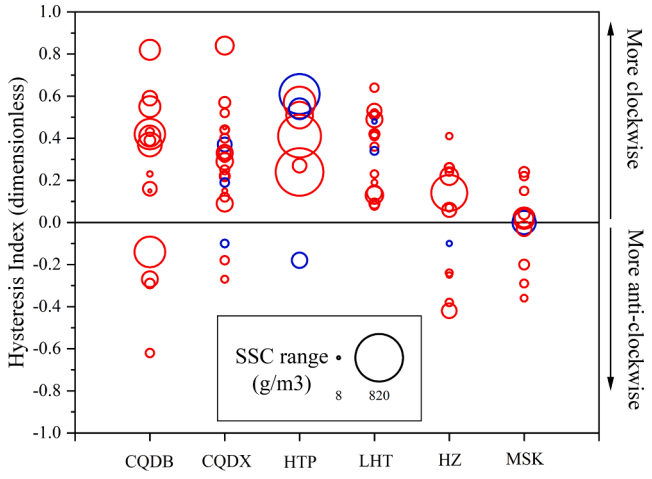

Fig. 5. maximum suspended sediment concentrations (circle size: magnitude of sediment response) and hysteresis index (HI_{new}) for storm events during wet season (May to September) in red circles and dry season in blue circles in six hydrological stations from 2017 to 2018.

(May–September) accounted for more than 90% of hysteresis loops in all basins, and the wet-season SSC value was significantly higher than that in the dry season.

Fig. 6 shows all hysteresis types and their SS load ratios for the six hydrological stations. The SS load proportion does not strongly depend on the proportion of the loop type. For CQDB, the clockwise loops accounted for 60% of events and contributed 72% of the SS load, while figure-8 loops accounted for 7% of events but contributed <1% of the SS load. CQDX and LHT are similar in that the proportion of SS load depends on the quantity, and both had only anti-clockwise and figure-8 hysteresis types. The proportion of CQDX clockwise SS events was 64%, while that of LHT was 56%, whereas figure-8 represented 46% of SS load for CQDX and 44% of SS load for LHT. In contrast, at HTP, the clockwise type accounted for 76% of events and 92% of SS load, with the figure-8 type accounting for 24% of events and only 8% of the total SS load. The distribution of the hysteresis types in HZ was relatively balanced: event proportions were 38% anti-clockwise, 31% clockwise, and 31% figure-8, whereas the SS load was 51% anti-clockwise, 30% clockwise, and 19% figure-8. MSK was different from other stations: figure-8 accounted for 64% of the total number of events and 75% of the total SS load, with the remainder being anti-clockwise.

3.3. Storm event SS controls

Fig. 7 shows the PCA (principal component analysis) loading map for each hysteresis types in each sub-basin. In this study, the potential influencing factors of storm events were divided into three principal components (Loading Principal 1, 2 and 3), which accounted for at least 78.6% of the variation.

Table 5 shows the absolute distance between potential control variables and SSC_{mean} in Fig. 7. The closer the distance, the stronger the control (Dominic et al., 2015; Tena et al., 2014). In CQDB, clockwise is the main hysteresis type, which is strongly controlled by rainfall intensity index (I_{10}, I_{30}, I_{mean}). Anti-clockwise was mainly affected by the antecedent precipitation (3, 5, 7, 10-day antecedent rainfall). CQDX, still predominantly clockwise, is mainly related to the antecedent precipitation and maximum discharge (Q_{max}), while figure-8 is mainly related to rainfall intensity index (I_{10}, I_{30}, I_{mean}) and flood intensity. PCA analysis showed that hysteresis in HTP seemed to be independent of any potential controls. For LHT, both the clockwise and figure-8 types are influenced by rainfall intensity and total event precipitation, but clockwise is more dependent on rainfall duration, whereas figure-8 is more dependent on flood intensity. Due to the existence of the Qingshan reservoir, the hysteresis type in HZ is greatly disturbed by human activities (Reservoir drainage and storage). For MSK, figure-8 is positively related to rainfall intensity, flood intensity and maximum discharge, whereas anti-clockwise is mainly controlled by flood intensity.

4. Discussion

4.1. Characteristics of annual sediment transport in karst basins

Due to the special geological conditions, soil erosion and sediment transport in karst areas are more dependent on continuous rainfall than that in non-karst areas. From 2017 to 2018, storms during the wet season (May–September) accounted for 89% of events and 98% of total SS load, but they were not linearly dependent on rainfall (total rainfall during the two rainy wet seasons accounted for 67%). Under the action of differential karst dissolution, the topography of the epikarst zone is highly variable. Surface runoff only occurs under the condition of high rainfall, which is manifested as the mechanism of saturation-excess runoff (Peng and Wang, 2012). The epikarst zone plays a dominant role in the regulation and storage of rainfall and water (33–63%). Its hydrological regulation and storage function has a great range of variation, and is mainly controlled by the water content in the early stage, but less affected by rainfall intensity (Fu et al., 2016). As a result, a

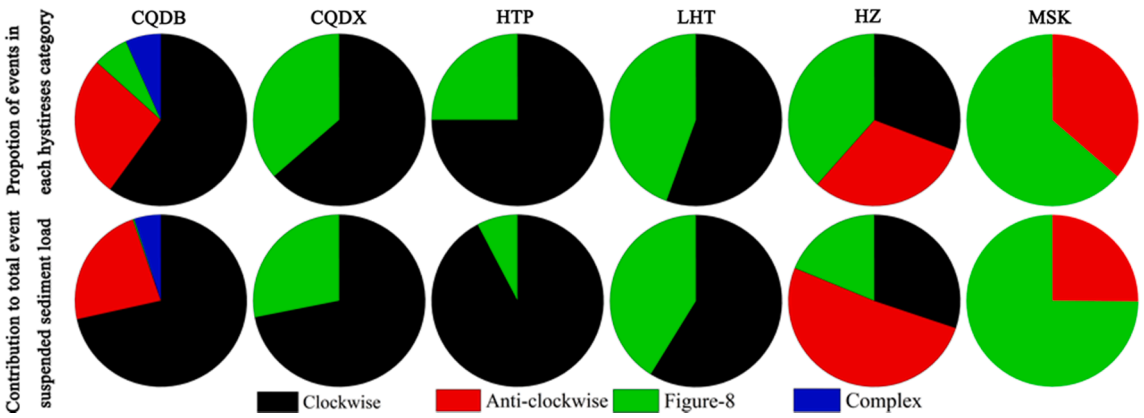

Fig. 6. Proportion of events categorized by hysteresis type (above), and the contribution of hysteresis type to total event load over monitoring period (below) in six hydrological stations.

single rainfall event does not threaten soil erosion in this area, while continuous rainfall has a disproportionate effect on soil erosion or sediment transport.

It is worth noting that the suspended sediment transport modulus of the basins in this study (0.8–6.6 Mg km^{-2} a^{-1}; Table 4) is far lower than that of non-karst areas. For example, the average annual sediment yield of a watershed in the north of the Loess Plateau is 1061–1736 Mg km^{-2} a^{-1} (Zhao et al., 2017). The annual soil erosion modulus of a basin in the black soil area of northeast China is about 800 Mg km^{-2} a^{-1} (Fang et al., 2013). Nonetheless, the risk of soil erosion in karst basins is not low. It takes 2000–8000 years to dissolve 25 m of pure carbonate rock and form 1 cm of soil (Jiang et al., 2014). If the soil formation rate is taken as the tolerance of soil loss, many research results show that the allowable loss rate in karst area is 0.2 to 55 Mg km^{-2} a^{-1}, with an average of 4.3 Mg km^{-2} a^{-1} (Cao et al., 2020; Jiang et al., 2014). This means that attention must be paid to the prevention and control of soil erosion in karst basins.

4.2. Hydrology connectivity and sediment availability

Q-SSC hysteresis type is fundamentally determined by geomorphology and ground substance component (GSC). The geomorphic characteristics determine the water source connectivity, while ground substance component determines the sediment availability. Table 3 shows the possible causes of each hysteresis category. In general, the clockwise hysteresis pattern is attributed to a rapid response where the distance between the sediment source and outlet is short. This pattern reflects rapid erosion and depletion of sediment in the stream network, because of a limited supply of readily available sediment for transport. Conversely, the anti-clockwise hysteresis pattern is often interpreted as sediment from more distant sources (related to extended travel time) (De Girolamo et al., 2015; Sun et al., 2016; Tena et al., 2014).

The geomorphology of a watershed affects the energy fluxes, mass movement, and water and sediment dispersion within the watershed (Zhang et al., 2015). Drainage density is an important index of geomorphology, which has a positive correlation with annual sediment yield (Li et al., 2019, Lane et al., 1997). Topographic relief influences the distribution of rivers and erosion characteristics of the basin. Generally speaking, the greater the topographic relief, the greater the potential energy of water and the stronger erosion capacity, thus the higher the suspended sediment concentration (Zhang et al., 2015, De Vente et al., 2011).

Ground substance component (GSC) is the material basis of sediment, including lithology, soil and vegetation, etc. In the karst area of southwest China, the sediment yield is closely related to the characteristics of lithology (Jiang et al., 2014). Fissures, conduits, and channels were extensively developed on limestone hillsides, resulting in high surface water leakage and low runoff coefficient (Peng and Wang 2012). Therefore, the wider the limestone coverage, the less runoff and less sediment transported by the surface river. However, the epikarst zone is not developed in the dolomite slope, with thin and uniform soil, and poor water holding capacity (Jiang et al., 2014). Hence, the sediment loss in the area dominated by dolomite is low. Good vegetation cover can conserve water and consolidate soil, so there is a negative correlation between vegetation cover and sediment transport (Braud et al., 2001; Ouyang et al., 2010). It should be noted that gully activity is not correlated with the percentage of total vegetation cover, but with the percentage of cover of low vegetation in the gully floor (Rey, 2003). This highlights the importance of spatial distribution of forest vegetation in reducing sediment yield at the gully outlet.

In this study, CQ belongs to the peak-cluster depression landform. The SS load at CQDB was dominated by positive HI_{new} (clockwise hysteresis), suggesting sediments were scour-derived. The project of returning farmland to forest greatly increased vegetation coverage in CQ basin, reduced the artificial disturbance of limestone slope land, and effectively controlled the soil erosion on the slopes (Cao et al., 2020). The sediment of CQDB should mainly come from low-lying paddy field. Peak-cluster valley occupies a large area of HTP sub-basin. Although 92% of the SS load in HTP basin is controlled by clockwise hysteresis, the event indicators (SSC_{mean}) are independent of other variables in PCA loading diagrams (Fig. 7). This shows that the Q-SSC relationship of HTP do not change significantly due to external conditions such as rainfall. Vegetation in upstream of HTP is mainly forest shrubs and grassland, which reduces the hydrological connectivity of the upstream surface (Mellander et al., 2015). The lower reaches are peak-forest plain (accounting for 24% of the total area of HTP), with flat terrain. A large amount of paddy soil and thick layer of loess are distributed around the river course, and the vegetation is dominated by crops (Fig. 2 (C)). It can be inferred that the source area of HTP sediment is mainly in the lowlands downstream. HTP was also marked by storm events with two SSC peaks (Fig. 6). The first peak was very early and short, which may be related to the lack of river power in the early stage, resulting in a small amount of coarse sediment deposited on the riverbed (Oeurng et al., 2010). In HZ, the total SS load is mainly controlled by anti-clockwise type flood (51% of the total SS load), which is related to Qingshan Reservoir. Reservoirs can store water, reduce the flood peak discharge and change the annual runoff distribution (Oeurng et al., 2010). The second major type of hysteresis in HZ is clockwise, where sediment is mainly proximally derived. In contrast to HTP and CQ, the lithology is dolomite from Qingshan Reservoir to HZ (Fig. 2B). Although loess and paddy soil are distributed around the river channel, large areas of grassland and artificial forest land are exposed. These conditions suggest that the proximal source of HZ sediment is bank erosion.

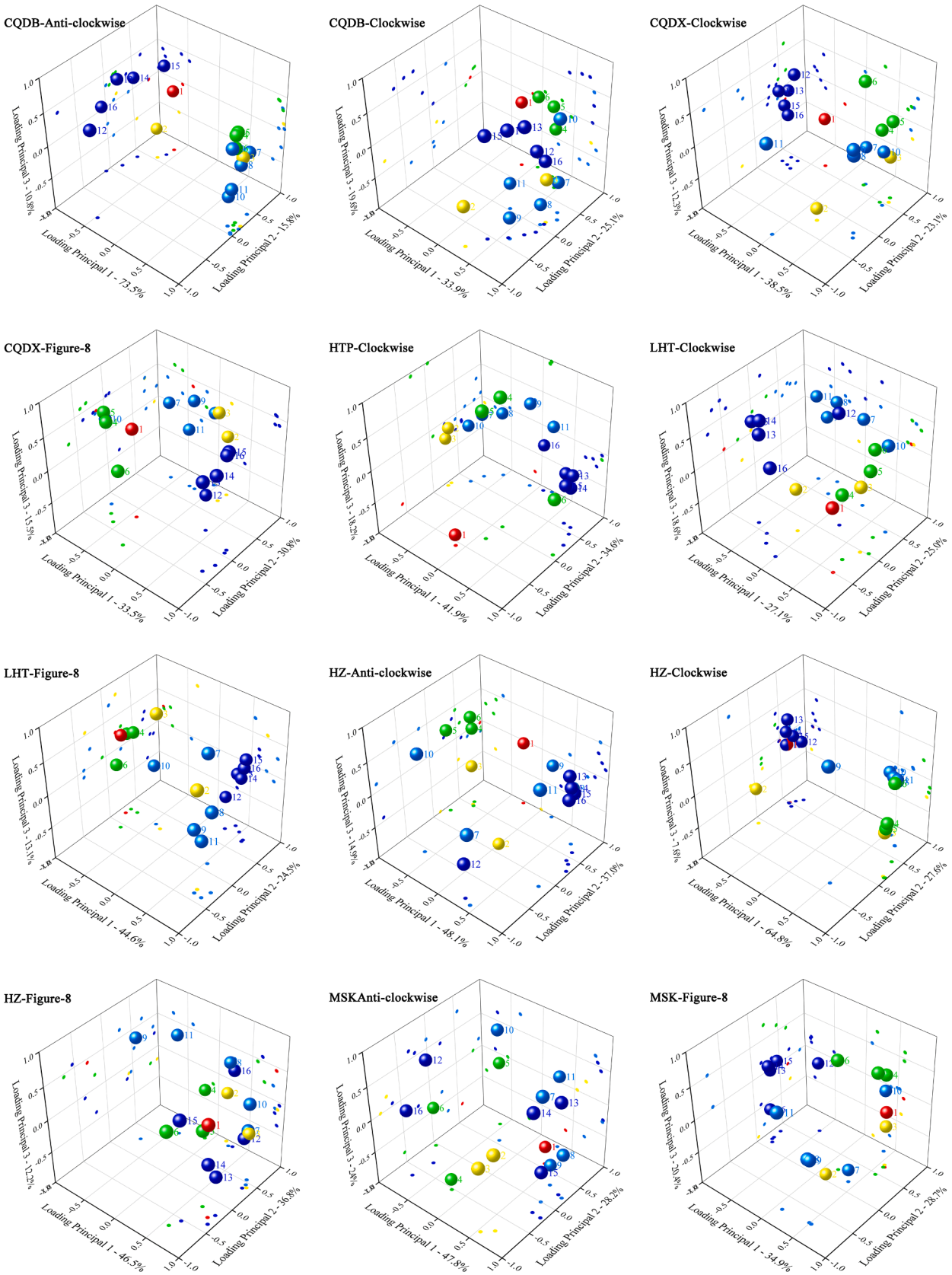

Fig. 7. Determination of controls on SSC_{mean} using PCA loading diagrams. 1 (the red ball): SSC_{mean}, 2: duration of rainfall event (hour), 3: total event precipitation (mm), 4: maximum precipitation intensity at 10 min, 5: maximum precipitation intensity at 30 min, 6: mean precipitation intensity, 7: maximum discharge (m^3/s), 8: total event discharge (m^3), 9: event duration, 10: flood intensity (($Q_{max} - Q_{min}$)/ time of rise), 11: runoff coefficient, from 12 to 16: antecedent rainfall at 1, 3, 5, 7 and 10 days before event initiation (mm).

Table 5
Absolute distance between potential control variables and SSC_{mean} in the PCA loading map.

	T_{rain}	P	I_{10}	I_{30}	I_{mean}	Q_{max}	Q_{total}	T	flood intensity	runoff coefficient	Antecedent rainfall				
											1-d	3-d	5-d	7-d	10-d
CQDB anti-clockwise	0.55	1.68	1.68	1.65	1.73	1.55	1.71	1.76	1.68	1.76	1.66	0.85	0.60	0.49	0.98
CQDB clockwise	1.68	1.16	0.61	0.48	0.27	1.18	1.31	1.51	1.13	1.02	1.30	1.47	1.52	1.56	1.15
CQDX clockwise	1.18	1.07	1.05	1.12	1.06	0.65	1.37	1.51	1.05	1.56	0.73	0.58	0.68	0.54	0.47
CQDX figure-8	1.30	1.08	0.35	0.39	0.58	0.91	1.19	0.92	0.42	1.02	1.22	1.27	1.31	1.28	1.28
HTP clockwise	1.40	1.3	1.9	1.8	1.39	1.60	1.6	1.86	1.44	1.80	1.53	1.60	1.5	1.53	1.61
LHT clockwise	0.92	0.47	0.24	0.60	0.86	1.31	1.70	1.45	1.01	1.78	1.10	1.17	1.29	1.40	0.83
LHT figure-8	1.72	0.78	0.16	0.10	0.38	1.50	1.84	1.75	0.55	1.87	1.52	1.51	1.57	1.61	1.60
HZ anti-clockwise	1.31	0.75	0.68	1.02	0.80	1.99	1.01	0.48	1.66	1.66	1.94	1.28	1.32	1.14	1.41
HZ clockwise	0.69	1.86	1.88	1.88	1.76	1.47	1.61	1.82	1.39	1.60	0.19	0.46	0.21	0.14	0.01
HZ figure-8	1.56	0.91	1.60	0.32	0.48	0.93	1.34	1.69	0.86	1.61	0.92	0.82	0.50	0.34	1.35
MSK anti-clockwise	1.61	1.60	1.25	1.22	1.49	1.52	0.78	0.40	1.64	0.93	1.95	1.30	1.55	1.07	1.84
MSK figure-8	1.13	0.26	0.56	0.71	1.00	0.88	1.35	1.35	0.32	1.59	1.12	1.56	1.58	1.54	1.56

4.3. Effects of storm event characteristics on suspended sediment yield

In areas dominated by hydraulic erosion, rainfall and runoff are the main natural driving factors of soil erosion. Soil erosion in karst areas must be different from that in non-karst areas because of the "dual structure". To obtain the main driving factors of sediment transport among basins with different landforms and ground substance component, a total of 16 hydrological and rainfall indicators were taken into consideration (Table 5).

The main external factors affecting sediment transport in CQ are rainfall intensity (I_{30}) and antecedent precipitation. CQ are mainly composed of peak-cluster depression, with seasonal surface river, and developed epikarst zone (Fig. 2 (D)). The potential energy of groundwater is large, and the water (precipitation, surface and ground water) transformation are rapid. The epikarst zone absorbs a considerable part of precipitation via solution-enhanced rock joints, fissures and pipes (Williams, 2008). However, the antecedent precipitation will make part of epikarst be filled with rainwater, which may cause erosion with less precipitation in the later stage. For example, In the case of antecedent precipitation, a single rainfall greater than 10 mm may cause significant water stage changes in underground rivers. However, in the absence of antecedent precipitation situation, 23 mm precipitation is needed to achieve the same effect (Cao et al., 2020). The surface sediment transport is controlled by rainfall intensity, and the surface water can enter the underground system through sinkholes, which makes the sediment transport in underground river also under the control of rainfall intensity. Fingerprint tracing shows that surface sediment accounts for 38% of the sediment in underground rivers, which supports this view (Cheng et al., 2020).

PCA analysis cannot give the main control factors of HTP sediment transport, this also shows that the Q-SSC of HTP is determined by the internal characteristics of the basin: ground substance component (GSC) and geomorphology. LHT is similar to CQDX, in which, intense floods connect surface water with the underground river through sinkholes, thus providing another important sediment source. The distribution of landforms and soils in LHT watershed is similar to that of HTP, but surface rivers in the upper and middle reaches of the LHT exit the basin in the northwest, which may explain the low annual sediment transport modulus (0.8–1.3 Mg km^2 a^{-1}) of the LHT station.

MSK is the total outlet of groundwater in Houzhai basin, which has complex geomorphology, soil and land use units. Therefore, the sediment transport characteristics of MSK represent the general sediment transport characteristics of underground rivers in southwest karst area. The main external controlling factors of MSK sediment transport are precipitation, event duration and total event discharge. The average value of HI_{new} for MSK is −0.06, so the peak of the SSC tends to lag the peak of Q. The contribution of figure-8 to SS load (75%) is positively correlated with precipitation intensity, flood intensity and maximum discharge. There is a large amount of paddy soil exposed at the proximal end, and high-intensity rainfall can easily divert proximal sediment into the subsurface through sinkholes (Fig. 2). During the wet season (May–September), the elevated water level of Qingshan Reservoir caused surface water that should have flowed into the reservoir to be diverted into the subsurface conduit network. That water instead flowed to MSK via Maokeng (Fig. 2D), which is another important distal sediment source of MSK. Similarly, Barna et al. (2020) observed temporary flow reversals within the conduit network between LHT and MSK. Anti-clockwise hysteresis at MSK (25%) is mainly controlled by event duration. Barna et al. (2020) found that the groundwater velocity within the conduit network was 2–3 km/d in summer and 0.4–2 km/day in winter. Because the maximum conduit length in the basin is 16 km, the travel time from the upstream end of the basin to MSK is 5–8 days. Therefore, the longer the flood duration, the higher the proportion of distal sediment, which shows as anti-clockwise hysteresis.

4.4. Watershed management based on sediment sources and connections

Reducing soil loss and sediment transport requires management strategies based on catchment characteristics, that is, availability and regional connectivity of sediment sources. It is important to note that the contribution of the sediment rather than the frequency of the hysteresis type must be used to prioritize the management strategy.

In the CQ river basin, surface soil erosion mainly comes from paddy fields, and the remote hillsides are not the focus of soil and water conservation. Special attention should be paid to the influx of flood water into the valley during heavy rains, and to the accumulation of rainwater in the farmland itself. Therefore, building drainage facilities along the perimeter of farmland can effectively prevent soil erosion on the surface. CQDX has a large amount of sediment from surface water pouring into the sinkhole during the rainstorm, so walls and other protective works around the sinkhole should be considered. The geomorphology and other conditions in the HTP watershed effectively reduce the risk of soil loss from upstream. However, the thick layer of loess distributed around the river channel can output a large amount of sediment after the surface passage is activated by rainfall exceeding the infiltration capacity. Large-scale conversion of farmland to grass would be effective in reducing sediment transport, but in HTP, where agricultural productivity is prioritized, this is impractical. Thus, planting shelterbelts along river channels, increasing surface roughness, and adding temporary sediment control measures, such as sediment fences, may be practical solutions in HTP. Hydraulic engineering can effectively change regional hydrological conditions, such as the Qingshan Reservoir, which reduces HZ SS load. However, the reservoir may be affected by siltation over time. Riverbank erosion is the main sediment source in HZ, and sediment can be reduced by hardening the riverbank and increasing its stability. MSK and LHT are typical examples of underground sediment transport. Both show the characteristics of multiple sediment sources, which is related to the complexity of underground structure and the

seasonal connectivity, and they also exhibit connectivity to surface sediment. Subsurface soil leakage is a prominent feature in karst areas. Due to its concealment and complexity, more research is needed in the future.

Climate change prediction shows that the increasing frequency of floods in southwest China will aggravate soil erosion and sediment transport (He et al., 2011). The karst mountainous area is large, the available land is scattered, the soil layer is thin, and there is a lack of available groundwater, which is not conducive to agricultural production. Changing the land-use structure and ecological development mode are important strategies to improve the environment in the future.

5. Conclusions

This 2-year study used a hysteresis index of discharge and suspended sediment data, combined with the basin's inherent geological characteristics, to assess sediment sources and transport mechanisms at six sites in an agricultural karst watershed of southwest China, so that targeted sediment management measures can be developed. The conclusions can be summarized as follows:

The sediment transport modulus of the river in this karst basin is very low (0.8–6.6 Mg km^2 a^{-1}). Due to the developed epikarst zone in this area, sediment transport depends on continuous rainfall, and the amount of sediment transport in rainy season accounts for more than 90% of the total annual sediment transport. The proportion of sediment transport in underground rivers ranges from 17% to 81%, which also reflects the special phenomenon of soil leakage in karst area. Ground substance component (GSC) is the material basis of soil erosion, and geomorphology characteristics determine the hydrology connectivity in a basin. These two conditions regulate the discharge-suspended sediment hysteresis type. External conditions such as rainfall and pre-watershed soil moisture will further characterize the river's Q-SSC type. Discharge-suspended sediment concentration hysteresis analysis has proved to be a simple and efficient method to understand the sediment sources and flow pathways in many other areas, and it also can provide a reference for soil and water conservation decision-making in karst areas.

CRediT authorship contribution statement

Le Cao: Conceptualization, Methodology, Software, Investigation, Writing - original draft. **Shuang Liu:** Methodology, Data curation, Resources. **Shijie Wang:** Validation, Formal analysis, Data curation, Supervision, Funding acquisition, Project administration. **Qianyun Cheng:** Resources, Data curation. **Alan E. Fryar:** Writing - review & editing, Supervision. **Lin Zhang:** Resources, Data curation. **Zhicai Zhang:** Resources, Data curation. **Fujun Yue:** Resources, Data curation. **Tao Peng:** Validation, Formal analysis, Data curation, Funding acquisition, Project administration, Supervision, Writing - review & editing.

Declaration of Competing Interest

The authors declare that they have no known competing financial interests or personal relationships that could have appeared to influence the work reported in this paper.

Acknowledgments

This work was supported by the National Key Research and Development Program of China [2016YFC0502602]; The "Strategic Priority Research Program" of the CAS [XDB4002020104]; The National Natural Science Foundation of China [41571130074, U1612441, 42077317]; The Bureau of International Cooperation, CAS [132852KYSB20170029]. The 2020 West Light Foundation of the CAS. Thanks to those anonymous reviewers, who provided thoughtful comments that improved the manuscript.

References

Bai, Z.G., Wan, G.J., 1998, Study on erosion rate and environmental effect of carbonate rock area in Guizhou Province. J. Soil Erosion Soil and Water Conserv. 1, 1–7,46 (in Chinese).

Barna, J.M., Fryar, A.E., Cao, L., Currens, B.J., Zhu, C., 2020. Variability in groundwater flow and chemistry in the houzhai karst basin, guizhou province, china. Environ. Eng. Geosci. 26 (3).

Belmont, P., Willenbring, J.K., Schottler, S.P., Marquard, J., Kumarasamy, K., Hemmis, J. M., 2014. Toward generalizable sediment fingerprinting with tracers that are conservative and nonconservative over sediment routing timescales. J. Soils Sediments 14, 1479–1492.

Braud, I., Vich, A.I.J., Zuluaga, J., Fornero, L., Pedrani, A., 2001. Vegetation influence on runoff and sediment yield in the Andes region: observation and modelling. J. Hydrol. 254, 124–144.

Cao, L., Wang, S., Peng, T., Cheng, Q., Zhang, L., Zhang, Z., Yue, F., Fryer, A.E., 2020. Monitoring of suspended sediment load and transport in an agroforestry watershed on a karst plateau, Southwest China. Agric. Ecosyst. Environ. 299, 106976.

CAO Jian hua, YUAN Dao xian, PAN Gen xing, 2003, Some soil features in karst ecosystem. Adv. Earth Sci. 18(1), 37–044 (in Chinese).

Cheng, Qianyun, Wang, Shijie, Peng, Tao, Cao, Le, Zhang, Xinbao, Buckerfield, Sarah J., Zhang, Yusheng, Collins, Adrian L., 2020. Sediment sources, soil loss rates and sediment yields in a Karst plateau catchment in Southwest China. Agric. Ecosyst. Environ. 304, 107114. ISSN 0167-8809.

Chen, H., Oguchi, T., Wu, P., 2017, Assessment for soil loss by using a scheme of alterative sub-models based on the RUSLE in a Karst Basin of Southwest China. J. Integr. Agric. 16, 377–388.

De Girolamo, A.M., Pappagallo, G., Lo Porto, A., 2015. Temporal variability of suspended sediment transport and rating curves in a Mediterranean river basin: The Celone (SE Italy). CATENA 128, 135–143.

De Vente, J.D., Verduyn, R., Verstraeten, G., Vanmaercke, M., Poesen, J., 2011. Factors controlling sediment yield at the catchment scale in NW Mediterranean geoecosystems. J. Soils Sediment. 11, 690–707.

Dominic, J.A., Aris, A.Z., Sulaiman, W.N.A., 2015. Factors controlling the suspended sediment yield during rainfall events of dry and wet weather conditions in a tropical urban catchment. Water Resour. Manage. 29, 4519–4538.

Eder, A., Strauss, P., Krueger, T., Quinton, J.N., 2010. Comparative calculation of suspended sediment loads with respect to hysteresis effects (in the Petzenkirchen catchment, Austria). J. Hydrol. 389, 168–176.

Fang, H.Y., Sheng, M.L., Tang, Z.H., Cai, Q.G., 2013. Assessment of soil redistribution and spatial pattern for a small catchment in the black soil region, Northeastern China: Using fallout 210Pbex. Soil Tillage Res. v. 133, 85–92.

Fu, Z., Chen, H., Xu, Q., Jia, J., Wang, S., Wang, K., 2016. Role of epikarst in near-surface hydrological processes in a soil mantled subtropical dolomite karst slope: implications of field rainfall simulation experiments. Hydrol. Process. 30, 795–811.

Gao Huaduan, Li Rui, 2006. Characteristics of soil and water loss based on geological background in Guizhou province. Sci. Soil Water Conserv. 26–32 (in Chinese).

Gippel, C.J., 1995. Potential of turbidity monitoring for measuring the transport of suspended solids in streams. Hydrol. Process. 9, 83–97.

Jiang, Z., Lian, Y., Qin, X., 2014. Rocky desertification in Southwest China: Impacts, causes, and restoration. Earth Sci. Rev. 132, 1–12.

Krueger, T., Quinton, J.N., Freer, J., Macleod, C.J.A., Bilotta, G.S., Brazier, R.E., Butler, P., Haygarth, P.M., 2009. Uncertainties in data and models to describe event dynamics of agricultural sediment and phosphorus transfer. J. Environ. Qual. 38, 1137–1148.

Lane, L.J., Hernandez, M., Nichols, M., 1997. Processes controlling sediment yield fromwatersheds as functions of spatial scale. Environ. Model Softw. 12, 355–369.

Langlois, J.L., Johnson, D.W., Mehuys, G.R., 2005. Suspended sediment dynamics associated with snowmelt runoff in a small mountain stream of Lake Tahoe (Nevada). Hydrol. Process. 19, 3569–3580.

Li, S., Liu, C., Li, J., Lang, Y., Ding, H., Li, L., 2010. Geochemistry of dissolved inorganic carbon and carbonate weathering in a small typical karstic catchment of Southwest China: Isotopic and chemical constraints. Chem. Geol. 277, 301–309.

Li, Y., Bai, X., Zhou, Y., Qin, L., Tian, X., Tian, Y., Li, P., 2016. Spatial-Temporal Evolution of Soil Erosion in a Typical Mountainous Karst Basin in SW China, Based on GIS and RUSLE. Arab. J. Sci. Eng. 41, 209–221.

Li, Z., Xu, X., Zhu, J., Xu, C., Wang, K., 2019. Effects of lithology and geomorphology on sediment yield in karst mountainous catchments. Geomorphology 343, 119–128.

Li, Zhenwei, Xianli, Xu., Zhang, Yaohua, Wang, Kelin, 2020. Fingerprinting sediment sources in a typical karst catchment of southwest China. Int. Soil Water Conserv. Res. 8 (3), 277–285. ISSN 2095-6339.

Lloyd, C.E.M., Freer, J.E., Johnes, P.J., Collins, A.L., 2016. Technical Note: Testing an improved index for analysing storm discharge–concentration hysteresis. Hydrol. Earth Syst. Sci. 20, 625–632.

Mellander, P., Jordan, P., Shore, M., Melland, A.R., Shortle, G., 2015. Flow paths and phosphorus transfer pathways in two agricultural streams with contrasting flow controls. Hydrol. Process. 29, 3504–3518.

Ouyang, W., Hao, F., Skidmore, A.K., Toxopeus, A.G., 2010. Soil erosion and sediment yield and their relationships with vegetation cover in upper stream of the Yellow River. Sci. Total Environ. 409, 396–403.

Oeurng, C., Sauvage, S., Sánchez-Pérez, J., 2010. Dynamics of suspended sediment transport and yield in a large agricultural catchment, southwest France. Earth Surf. Proc. Land. 35, 1289–1301.

Peng, T., Wang, S., 2012. Effects of land use, land cover and rainfall regimes on the surface runoff and soil loss on karst slopes in southwest China. CATENA 90, 53–62.

Saleh, A., 2008. Evaluating long-term annual sediment yield estimating potential of GIS interfaced MUSLE model on two micro-watersheds.: Pakistan journal of biological sciences. PJBS v, 11.

Sherriff, S.C., Rowan, J.S., Melland, A.R., Jordan, P., Fenton, O., HUallacháin, D.Ó., 2015. Investigating suspended sediment dynamics in contrasting agricultural catchments using ex situ turbidity-based suspended sediment monitoring. Hydrol. Earth Syst. Sci. 19, 3349–3363.

Sherriff, S.C., Rowan, J.S., Fenton, O., Jordan, P., Melland, A.R., Mellander, P., HUallacháin, D.Ó., 2016, Storm event suspended sediment-discharge hysteresis and controls in agricultural watersheds: implications for watershed scale sediment management. Environ. Sci. Technol. 50, 1769–1778.

Sun, L., Yan, M., Cai, Q., Fang, H., 2016. Suspended sediment dynamics at different time scales in the Loushui River, south-central China. CATENA 136, 152–161.

Tena, A., Vericat, D., Batalla, R.J., 2014. Suspended sediment dynamics during flushing flows in a large impounded river (the lower River Ebro). J. Soils Sediments 14, 2057–2069.

Vercruysse, K., Grabowski, R.C., Rickson, R.J., 2017. Suspended sediment transport dynamics in rivers: Multi-scale drivers of temporal variation. Earth Sci. Rev. 166, 38–52.

Vigiak, O., Malagó, A., Bouraoui, F., Vanmaercke, M., Obreja, F., Poesen, J., Habersack, H., Fehér, J., Grošelj, S., 2017. Modelling sediment fluxes in the Danube River Basin with SWAT. Sci. Total Environ. v. 599–600, 992–1012.

Williams, P., 2008. The role of the epikarst in karst and cave hydrogeology: a review. Int. J. Speleol. 37, 1–10.

Yue, F., Li, S., Liu, C., Lang, Y., Ding, H., 2015. Sources and transport of nitrate constrained by the isotopic technique in a karst catchment: an example from Southwest China. Hydrol. Process. 29, 1883–1893.

Yan, H., Zhang, J.X., Li, B.Y., Zhu, C.L., 2021. Crack propagation patterns and factors controlling complex crack network formation in coal bodies during tri-axial supercritical carbon dioxide fracturing. Fuel 286.

Zhao, G., Mu, X., Han, M., An, Z., Gao, P., Sun, W., Xu, W., 2017. Sediment yield and sources in dam-controlled watersheds on the northern Loess Plateau. CATENA 149, 110–119.

Li, Zhenwei, Xu, Xianli, Chaohao, 2017, Monthly sediment discharge changes and estimates in a typical karst catchment of southwest China: Journal of Hydrology.

Gao, X., Cai, X.F., Wang, J., Hu, G.F., 2013. Distributed soil erosion estimation model for small karst watersheds. J. Mountain Sci. 31, 542–547 (in Chinese with English abstract).

He, J.Y., Zhang, M.J., Wang, P., Wang, S.J., Wang, X.M., 2011. Climate characteristics of the extreme drought events in Southwest China during recent 50 Years. Acta Geogr. Sin. 66, 1179–1190 (in Chinese with English abstract).

He, Yongbin, Zhang, Xinbao, Wen, Anbang, 2009. Discussion on karst soil erosion mechanism in karst mountain area in southwest China. Ecol. Environ. Sci. 018 (006), 2393–2398 (in Chinese with English abstract).

Rey, F., 2003. Influence of vegetation distribution on sediment yield in forested marly gullies. CATENA 50, 549–562.

Wang, L.C., Zhang, Y.Z., 2001. Karst conduit flow and its hydrodynamic characteristics—Houzhai River drainage basin in Puding, Guizhou, China, as an example. Chin. Sci. Bull. 46, 45–51.

Wang, S.J., Li, Y.B., Li, R.L., 2003. Karst rocky desertification: Formation background, Evolution and comprehensive taming. Quat. Sci. 657–666 (in Chinese with English abstract).

Zhang, X.B., Wang, S.J., He, X.B., Wang, Y.C., He, Y.B., 2007. Soil creeping in weathering crusts of carbonate rocks and underground soil losses on karst slopes. Earth Environ. 2007 (03), 202–206 (in Chinese with English abstract).

Zhang, H.Y., Shi, Z.H., Fang, N.F., Guo, M.H., 2015. Linking watershed geomorphic characteristics to sediment yield: Evidence from the Loess Plateau of China. Geomorphology 234, 19–27.